焊接逆变电源与涡流检测融合设计分析

谢宝忠[1]， 薛家祥[2]， 龙 鹏[2]， 杨向宇[1]， 杨 苹[1,3]， 陈铁群[2]
(1. 华南理工大学 电力学院，广州 510640; 2. 华南理工大学 机械与汽车工程学院，广州 510640;
3. 华南理工大学 广东省绿色能源技术重点试验室，广州 510640)

谢宝忠

摘 要: 根据焊接逆变电源与涡流检测的工作原理，在焊接逆变电源中加入涡流检测激励与接收部分的模拟信号处理电路，而涡流检测的数字信号处理部分则与焊接逆变电源共用，实现焊接逆变电源与涡流检测的融合设计. 焊接逆变电源主变压器输出的交流方波经过滤波后，以滤波器输出的正弦波作为涡流检测的激励信号，驱动涡流检测探头，涡流检测探头接收的信号经过放大、比较、检波及后续的数字信号处理进行缺陷判断，实现涡流检测. 结果表明，该融合系统能够在不影响焊接的条件下为逆变电源增加涡流检测功能.

关键词: 焊接逆变电源; 涡流检测; 融合设计
中图分类号: TG434.1+3 **文献标识码**: A **文章编号**: 0253-360X(2013)05-0017-04

0 序 言

焊接作为一种重要的加工手段广泛地应用于各个行业，焊接电源是焊接加工的核心设备，从早期的工频电源逐步升级为数字化逆变电源，逆变电源具有稳定、灵活、准确、可靠、快速的优点，容易实现自动化，生产效率高，可进行全位置焊接，节能效果好，比一般电源更能适合制造业发展的需要[1]. 数字化逆变电源是焊接加工领域中的一个重要研究课题，当前逆变式焊接电源主要以 IGBT 作为功率控制器件来提高主电路的可控性和可靠性; 控制系统从早期的模拟电路逐步升级为数字电路，如以 ARM 和 DSP 作为主控芯片的智能弧焊电源控制系统[2]; 利用自关断器件的脉冲宽度调制与脉冲频率调制混合模式的软开关控制方法[3]. 这些逆变式焊接电源通过数字系统处理焊接数据，控制整个焊接过程，使得数字控制的优势得以充分体现. 逆变式电源为焊接质量的改进提供了巨大帮助，但上述方式对于焊接加工质量而言均为开环形式，根据质量管理与质量控制理论[4]，高质量的产品要对产品生命周期的各个环节进行监控，对各种加工方式进行检测以构成质量控制的闭环结构，焊接加工、热处理等材料加工方法的检测主要采用无损检测技术.

在无损检测领域，涡流检测有着广泛的应用，其基本原理是在激励线圈中通以激励电流，导电体内会感应出涡流，导体材料的组织结构及缺陷等会影响检测线圈的阻抗，导致电流的幅值、相位等参数的改变. 涡流检测激励电流主要有单频、多频交流与脉冲等，检测信号包括幅值、相位等参数，通过幅值、相位等参数的处理实现缺陷的检测[5-8].

焊接逆变电源通过电力电子器件实现低频交流—直流—高频交流的转换，在直流—高频交流的逆变过程产生交流电流，这为涡流检测激励电流的实现提供了基础. 通过对焊接逆变电源中的交流方波进行滤波，为涡流检测提供激励电流，并对检测信号进行处理实现焊接与涡流检测的融合设计.

1 融合设计基础

1.1 焊接逆变电源原理

焊接逆变电源是将电网的三相 380 V 交流电源进行整流、滤波后，转换为低纹波 540 V 左右的直流，然后经 IGBT 和主脉冲变压器进行 DC-AC 逆变，产生 20 kHz 交流方波，再经二次整流变成直流，并经过电抗及电容的滤波作用，为焊接电弧负载提供所需能量[2]，图 1 为焊接逆变电源的结构框图.

在图 1 所示的结构图中，DSP 作为数字控制核

收稿日期: 2013-01-11
基金项目: 国家自然科学基金资助项目(50805053); 广东省自然科学基金资助项目(8451064101000263); 广东省绿色能源技术重点试验室资助项目(2008A060301002); 广东省科技攻关项目(2006B12401001,2004A11303001)

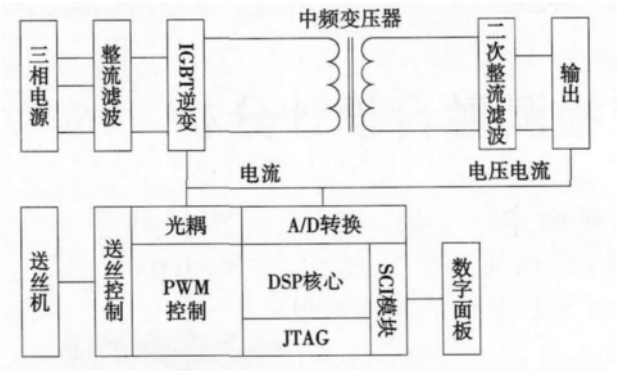

图 1 焊接逆变电源结构框图

Fig. 1 Structure diagram of welding inverter power

心，实现软开关的功能，输出的 PWM 由光耦隔离放大，驱动 IGBT 模块；焊接过程中的电流、电压等参数经 A/D 转换反馈到 DSP，构成控制系统的闭环结构；并将其它 PWM 输出作为 D/A 转换器，驱动送丝电路，调节送丝速度；数字面板通过 SCI 通讯模块实现人机交互；DSP 还实现逻辑控制、数据存储及管理等功能，实现全数字化控制[2].

1.2 涡流检测原理

涡流检测基于电磁感应原理，在涡流探头线圈中施以交变电流，所建立的交变磁场与导体相互感应导致线圈电压、相位与阻抗的改变. 当导体表面有缺陷或材质特征发生变化时，会影响涡流的强度和分布，并引起线圈电压、相位和阻抗的变化. 典型的涡流检测系统结构如图 2 所示.

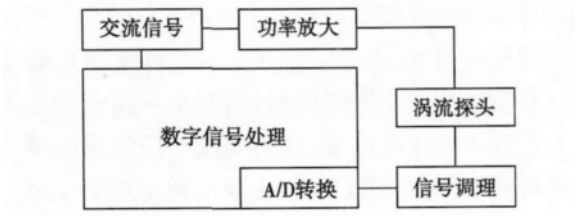

图 2 涡流检测系统结构图

Fig. 2 Structure diagram of eddy current testing system

在图 2 所示的涡流检测系统结构图中，交流信号通过振荡器或 DDS(direct digital synthesis)[3] 等方式产生；功率放大部分将交流信号进行放大以驱动涡流检测探头；探头通过交流电流的激励产生交变电磁场对材料进行检测，并输出检测信号；信号调理主要将探头输出的检测信号进行放大、滤波以及检波等处理，并将信号输出至 A/D 转换器进行采样，转换为数字信号，以进行后续的数字信号处理，将检测信号中的幅值、相位等参数提取出来，判断材料是否有缺陷的存在，并对缺陷进行评估.

2 融合设计

2.1 逆变电源与涡流融合设计

根据图 1、图 2 中焊接逆变电源与涡流检测的结构对比可以看出，焊接逆变电源的数字处理系统与涡流检测的数字信号处理单元部分作用一致，当前逆变电源的数字处理部分一般采用性能较高的 DSP，ARM 等嵌入式系统，具有较强的处理能力，可与涡流检测的数字信号处理功能一起实现. 涡流检测所需的交变激励电流由交变信号经功率放大驱动涡流检测探头，也可对焊接逆变电源中的交流方波进行滤波，把交变方波中的高次谐波滤除来驱动涡流检测探头. 由于焊接逆变电源中的交流方波本身有很强的驱动能力，滤波后可以直接驱动涡流探头，从而取消功率放大部分. 融合系统需增加涡流探头输出的信号调理单元.

根据以上分析，设计的融合系统结构如图 3 所示. 在图 3 所示的焊接逆变电源与涡流检测融合设计中，融合系统相对于焊接逆变电源增加的涡流检测模块包括将焊接逆变电源中频变压器二次侧输出的逆变方波进行滤波以及涡流检测信号的放大、滤波等信号调理两个硬件部分. 对调理后的信号进行的数字信号处理则由逆变电源中的 DSP 单元完成.

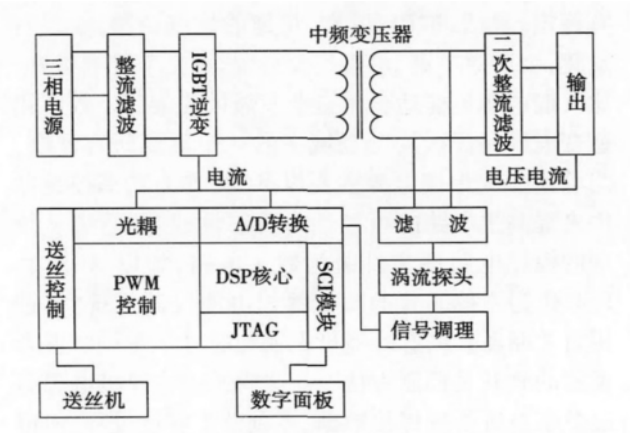

图 3 焊接逆变电源与涡流检测融合系统框图

Fig. 3 Structure diagram of welding inverter power and eddy current testing fusion system

2.2 涡流检测电路模块

逆变方波的滤波是将逆变电源中频变压器二次侧输出的 20 kHz 交流方波经过无源带通滤波器转换成正弦激励电流驱动涡流探头的激励线圈. 图 4 为逆变电源中频变压器二次侧输出的方波波形及其功率谱分布.

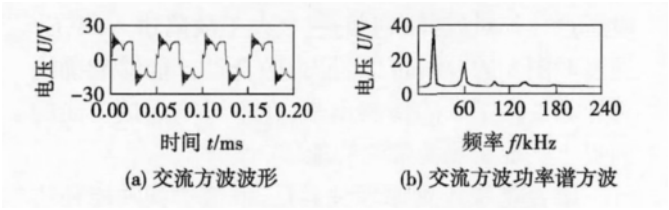

图 4　交流方波波形及其功率谱分布

Fig. 4　Alternative square waveform and its power spectrum distribution

从图 4b 功率谱分布可以看出,焊接逆变电源中交流方波的主要成分为 20 kHz 基频与 60 kHz 的 3 次谐波,将高次谐波滤除即可得到 20 kHz 的正弦交流信号用于驱动涡流检测探头.

逆变电源工作的过程中,交流方波不可避免地耦合到涡流检测模块中,干扰涡流检测,因此需要对交流方波进行抑制,降低其影响. 图 5 为涡流检测模块的硬件电路.

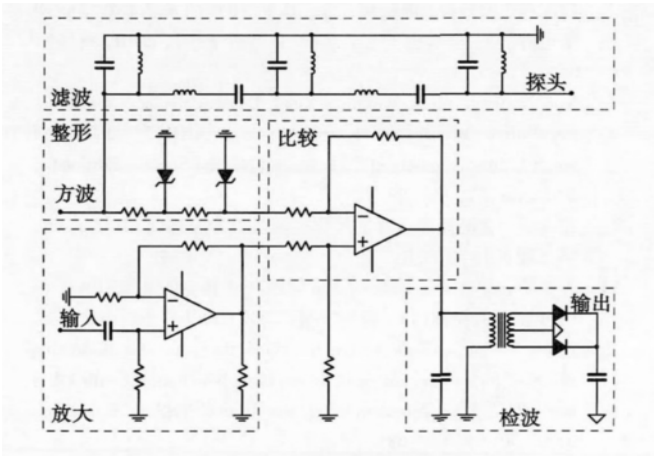

图 5　涡流检测模块电路图

Fig. 5　Eddy current testing circuit

在图 5 所示的涡流检测模块电路中,主要包括逆变方波的滤波以及接收信号的调理两大部分. 交流方波滤波通过无源带通滤波器实现,其通带中心频率为 20 kHz,带宽 8 kHz. 滤波器的输出驱动涡流探头,其电流为几十毫安,相对于逆变器几十安的输出驱动能力,可以忽略滤波器对焊接逆变电源负载的影响. 考虑到过高的滤波器阶数会导致滤波器设计的复杂,同时带来发热的问题,所以滤波器的阶数不宜过高,对此交流方波进行滤波,驱动涡流探头,得到如图 6 所示的波形.

从图 6a 可以看出,逆变电源的交流方波经过滤波后,高次谐波已经被滤除,其输出为正弦波; 图 6b 中的接收信号耦合有交流方波,需要对其进行调理,

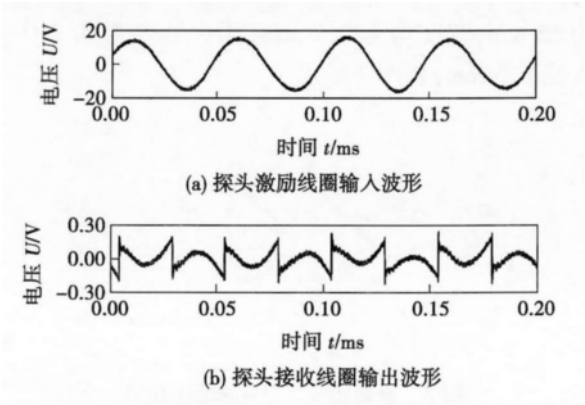

图 6　涡流检测探头激励与接收波形

Fig. 6　Exciting and received waveform of eddy current testing probe

以抑制其干扰. 涡流检测信号的调理主要有方波整形、输入信号放大、比较及检波等部分. 方波的整形是把逆变电源中不规整的 40 V 左右交流方波通过 15,2 V 两级齐纳二极管与分压电阻整形为幅值为 2 V 的规整方波,作为参考信号. 输入信号的放大是把涡流探头输出的检测信号放大供后续使用. 比较单元是把放大后的检测信号与方波参考信号通过减法器相减,抑制逆变电源中交流方波的干扰. 检波单元由变压器、二极管等构成,比较后的检测信号输入到变压器的原边,副边线圈具有中心抽头,连接参考地,两侧分别连接二极管构成全波整流,通过电容作为低通滤波器构成全波检波单元. 采用电容作为低通滤波器其效果不够理想,后续需要通过 A/D 转换器采样后进行数字滤波以及幅值、相位等检测参数的提取,进行缺陷的判断.

涡流检测探头的结构形式有多种,对涡流检测接收信号的处理要根据探头的结构形式与电路连接方式进行,对于绝对式探头,检测线圈输出的检测信号经电容耦合输入到信号调理单元放大器的同相输入端. 而对于差分式探头,可配备两个同样的信号调理单元,分别通过电容将两个信号耦合到放大单元,两组检波信号采样到 DSP 内部进行比较、分析处理.

3　结果分析

根据上述设计,在焊接逆变电源中增加涡流检测模块,两者分时工作互不干扰. 融合系统输入三相 380 V 工频交流电,焊接加工功能可正常实现,不需单独测试,下面仅对涡流检测模块进行测试.

涡流检测模块的测试通过人工缺陷样品实现,在金属铝样品上加工三个矩形槽 A,B,C,其长度均

为 35 mm，宽度均为 0.2 mm，深度分别为 0.2，0.5 以及 1.0 mm，如图 7 所示.

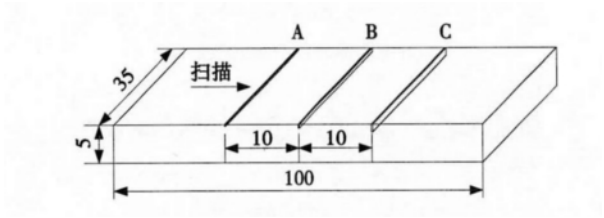

图 7 金属铝人工缺陷样品(mm)

Fig. 7 Aluminum artificial defect sample

采用绝对式探头对图 7 所示的样品进行扫描检测，得到如图 8 的检测与分析信号波形.

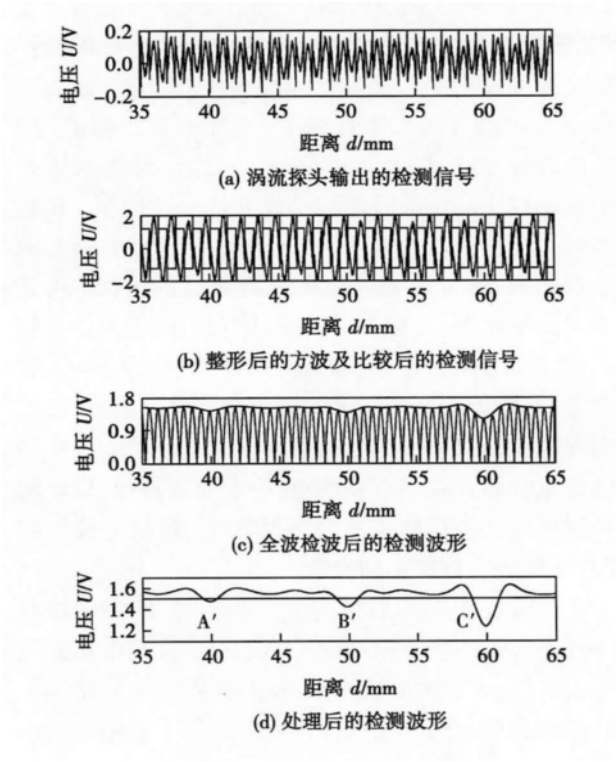

图 8 涡流检测模块各部分信号波形

Fig. 8 Analysis and processed signal waveform of eddy current testing module

图 8a 为探头接收线圈输出的检测波形，其中含有缺陷信息及交流方波的干扰；图 8b 为放大的接收信号图 8a 与经稳压管整形后的参考方波比较相减后的波形；图 8c 为图 8b 中的比较信号通过变压器及双二极管全波检波波形及其包络线. 对图 8c 中的检波信号滤波后，由 DSP 核心中的 A/D 转换单元采样，并经过数字滤波进一步处理，得到图 8d 中的检测曲线，图 8d 中的直线为通过试验确定的报警阀值，大小为 1.5 V，其中 A′，B′，C′三个低于 1.5 V 的电压点分别对应样品上的三个人工缺陷槽 A，B，C. 通过对图 8 的分析可以看出，融合设计能够准确地将样品的人工缺陷检测出来，在不影响焊接功能的前提下实现了涡流检测功能.

融合系统作为原理性验证，涡流检测功能还达不到专业涡流检测设备的性能，还需要进一步完善.

4 结 论

(1) 根据焊接逆变电源与涡流检测的原理，在焊接逆变电源中增加涡流检测模块，实现焊接加工与质量检测功能的融合.

(2) 焊接加工与涡流检测模块分时工作，可提高数字处理部分的利用率，分别实现焊接逆变电源与涡流检测的功能.

参考文献:

[1] 薛家祥，蒙万俊，熊丹枫，等. 基于 ARM 的多功能数字化逆变电源[J]. 华南理工大学学报(自然科学版)，2010，38(5)：95-99.
Xue Jiaxiang，Meng Wanjun，Xiong Danfeng，*et al*. Multifunctional digital inverter power supply based on ARM [J]. Journal of South China University of Technology (Natural Science Edition)，2010，38(5)：95-99.

[2] 黄文超. 智能弧焊电源的优化控制及其专家系统[D]. 广州：华南理工大学，2010.

[3] 张泰峰，周香全，郭秉楠. 高频感应焊接逆变电源 PWM 和 PFM 软开关控制[J]. 焊接学报，2009，30(8)：65-68.
Zhang Taifeng，Zhou Xiangquan，Guo Bingnan. Soft switching controlof high frequency induction welding power supply with PWM and PFM [J]. Transactions of the China Welding Instiution，2009，30(8)：65-68.

[4] Evans J R，Lindsay W M. 质量管理与质量控制[M]. 7 版. 北京：中国人民大学出版社，2010.

[5] HE D F，SHIWA M，JIA J P，*et al*. Multi-frequency ECT with AMR sensor [J]. Ndt & E International，2011，44(5)：438-441.

[6] HE Y，PAN M，LUO F，*et al*. Pulsed eddy current imaging and frequency spectrum analysis for hidden defect nondestructive testing and evaluation [J]. Ndt & E International，2011，44(4)：344-352.

[7] Kasai N，Matsuzaki S，Sakamoto T. Experimental and analytical study for detectability of the back-side flaws of flat ferromagnetic plates by RFECT [J]. Ndt & E International，2011，44(8)：703-707.

[8] Cao X H，Luo F L，Bai F T，*et. al*. A DDS waveform generator for electromagnetic non-destructive testing [J]. Measurement Technology and Intelligent Instruments VI Key Engineering Materials，2005(295-296)：661-666.

作者简介：谢宝忠，男，1977 年出生，博士，讲师. 主要从事无损检测技术与仪器方面的科研和教学工作. 发表论文 8 篇. Email：bobonx@scut.edu.cn

MAIN TOPICS, ABSTRACTS & KEY WORDS

Study on microstructure of fusing-brazing joint of aluminum to galvanized steel by pulsed DE-MIG welding SHI Yu[1], WANG Zhao[2], HUANG Jiankang[1], LU Lihui[2], FAN Ding[1] (1. State Key Laboratory of Gansu Advanced Nonferrous Metal Materials, Lanzhou University of Technology, Lanzhou 730050, China; 2. Key Laboratory of Nonferrous Metal Alloys of Ministry of Education, Lanzhou University of Technology, Lanzhou 730050, China). pp 1-4

Abstract: This paper put forward an arc welding method of pulsed DE-MIG welding, and introduced the basic principle of it. According to the characteristics and control requirements of this method, a pulsed DE-MIG welding experimental system based on rapid prototyping was established and it realized the dissimilar metal joining of aluminum and galvanized steel. The analysis of joint microstructure of aluminum and galvanized steel shows that Fe and Al atoms diffuse sufficiently in the intermediate interfacial region of joining of aluminum and galvanized steel. Ternary intermetallic compounds of lamellar $Fe_2Al_5Zn_{0.4}$ are generated. Rich-zinc zone is located at the weld toe, and is mainly composed of α-Al and β-Zn solid solution. Meanwhile, experiments of tensile and shear strength of overlap joints were conducted, and the results show that the maximum tensile strength is up to 186.73 MPa.

Key words: dissimilar metal; pulsed DE-MIG welding; intermediate interfacial region; rich-zinc zone

Study on combination process of resistance and laser spot welding for hot stamping boron steel CHEN Shujun, WANG Chao, HAO Sufeng, YU Yang (Advanced Manufacturing Technology for Automotive Structural Components Engineering Center of the Education Ministry, Beijing University of Technology, Beijing 100124, China). pp 5-8

Abstract: In order to avoid splash when large amount of heat of resistance spot welding is input for hot stamping high strength steel and meet the strict requirements for assembly under laser spot welding, a new welding process that is combination of resistance spot welding and laser spot welding is proposed. The welding joints were obtained through the combination of resistance and laser spot welding process. The microstructures of various regions for welding joints were analyzed with scanning electron microscopy. The micro-hardness distribution of welding joints was tested by micro-hardness testing. The mechanical properties of welded joints under different welding process were obtained by using universal tensile machine, and the fracture mode and fracture mechanism were analyzed. The results show that the welding area under process of combination of resistance and laser spot welding is composed of resistance welding zone and laser welding zone. The microstructure of laser nugget zone and base metal are lath martensite. The heat affected zone locates outside of laser ring and near the base metal, and the nugget of original resistance spot welding are tempering organization. The hardness of laser nugget zone is the same as that of base metal, and the hardness of softening zone corresponding to the tempering zone decreases to 60% of that of base metal. The softening zone outside of laser ring is the weak region for tensile-shear fracture. The obtained welding joints by this combination process have better load carrying capacity and toughness than those by individual resistance spot welding or laser welding.

Key words: hot stamping high strength steel; resistance spot welding; laser spot welding; mechanical property; failure mode

Study on heat-affected zone of TWIP steel after welding MI Zhenli, YANG Lin, LI Zhichao, JIANG Haitao (Metallargical Engineering Research Institute, University of Science and Technology Beijing, Beijing 100083, China). pp 9-12

Abstract: In this paper, microstructure and mechanical properties were analyzed on the heat-affected zone (HAZ) of the sheets obtained by applying laser beam and TIG welding. The result shows that microstructure of HAZ and fusion zone (FZ) becomes finer and distributes more uniformly and the elongation is significantly better than that of TIG welding. Microhardness of FZ is larger than that of the base metal. Grains of TIG welding in HAZ grow a lot, and microhardness is significantly reduced in the HAZ which leads to worse comprehensive performance.

Key words: twinning induced plasticity; tungsten inert gas welding; laser beam welding; heat affected zone

Mechanical property testing and analysis of T-joints in sandwich panels QIAO Jisen, GOU Ningnian, XU Xuemei, CHEN Jianhong (State Key Laboratory of Gansu Advanced Nonferrous Metal Materials, Lanzhou University of Technology, Lanzhou 730050, China). pp 13-16

Abstract: The deformation and failure of welded joints in the typical sandwhich panels have been studied by means of the shearing test and the T-joint bending test, combining with FEM simulation. The results show that during bending process, the welded joints between front panel and web panel are mainly subjected to shearing and bending moment parallel to the front panel. With load increasing, there is damage initiation at the weld root, along with a deep expanding cracking path. Aimed at the failure analysis of welded joints, experiments have a good agreement with numerical results.

Key words: sandwich panels; dual shearing; moment-rotation curve; mechanical property; finite element analysis

Design and analysis of welding inverter power and eddy current testing fusion system XIE Baozhong[1], XUE Jiaxiang[2], LONG Peng[2], YANG Xiangyu[1], YANG Ping[1,3], CHEN Tiequn[2] (1. School of Electric Power, South China University of Tech-

nology, Guangzhou 510640, China; 2. School of Mechanical & Automotive Engineering, South China University of Technology, Guangzhou 510640, China; 3. Guangdong Key Laboratory of Clean Energy Technology, Guangzhou 510640, China). pp 17-20

Abstract: A welding inverter power and eddy current testing fusion system is designed according to their operation principles. The analog signal processing circuit of the exciting and receiving parts in eddy current testing is added to welding inverter power, while the digital signal processing part in the eddy current testing is shared with that in welding inverter power. The alternative square wave from the main transformer in the inverter power is filtered, then the output sine signal of the filter drives the eddy current testing probe, and the received eddy current testing signal is amplified, compared and demodulated, and then it is digitized for the following digital signal processing to realize defect testing. The experiment results show that the fusion system can add eddy current testing function to inverter power without influence on welding.

Key words: welding inverter power; eddy current testing; fusion design

Modeling method for narrow gap MAG welding seam tracking based on rough sets LI Wenhang[1,2], SUN Dandan[1], YANG Feng[1], WANG Jiayou[1] (1. School of Material Science and Engineering, Jiangsu University of Science and Technology, Zhenjiang 212003, China; 2. Jiangsu Modern Shipbuilding Technology Co., Ltd., Zhenjiang 212003, China). pp 21-24

Abstract: For welding seam tracking of multi-layer single pass welding by narrow gap rotating arc MAG, an intelligent modeling method based on rough sets (RS) theory for seam deviation was put forward. First, workpiece was designed and processed to mimic multi-layer single pass welding groove, and enough experimental data were acquired under different deviations. Second, according to the simulation results of arc length and variation of experimental data, current signal was divided into 12 intervals in each rotating cycle. The mean value of each interval and differences between left and right intervals were computed to build decision table. Then after discretization and reduction for decision table, the knowledge model of "IF…THEN" form was obtained. At last the model was validated and compared with BP net model. It showed that the both models had similar predictive capability, and RS model precision could meet actual needs. Furthermore, RS model had better comprehensibility, and was useful to find potential laws between seam deviations and welding electrical signals from experimental data. The research was helpful for controller design.

Key words: narrow gap MAG welding; rough sets; rotating arc; seam deviation recognition

Prediction algorithm of molten pool width based on support vector machine during high-power disk laser welding WANG Teng[1,2], GAO Xiangdong[1] (1. School of Electromechanical Engineering, Guangdong University of Technology, Guangzhou 510006, China; 2. School of Computer, South China Normal University, Guangzhou 510630, China). pp 25-28

Abstract: As an important new laser processing technique, the high-power disk laser welding has been increasingly widely used in the manufacturing area. Aiming at the strong coupling multi-variable and real-time feedback requirements of the welding process, a new method by using support vector machine is proposed to predict the width of the molten pools. The performance of this model is validated by the test data. Meanwhile, analysis and comparison between the support vector machines and the BP neural network are conducted. Experiment results show that the support vector machine and the BP neural network both have a good training and single-step prediction ability and can be applied in the high-power disk laser welding process. However, in comparison with the BP neural network, the support vector machine is more suitable for high-power disk laser welding process. When N is 10, the prediction ability of SVR model reaches the optimum.

Key words: support vector machine regression; high-power disk laser welding; prediction of molten pool width

Study on effect of metal chlorides on penetration depth in A-TIG welding ZHANG Zhaodong, FAN Fuqun (Key Laboratory of Liaoning Advanced Welding and Joining Technology & School of Materials Science and Engineering, Dalian University of Technology, Dalian 116024, China). pp 29-32

Abstract: Three metal chlorides including KCl, $MnCl_2$ and $ZnCl_2$ were used as activating fluxes for the bead-on-plate A-TIG welding on magnesium alloy, aluminum alloy and Q235 steel. From the viewpoint of first ionization energy of the element, the effect of the three fluxes on the penetration depth was studied, and the mechanism was also discussed. The results indicated that metal element in the fluxes would move into the arc plasma and had influence on the arc state in the A-TIG welding process. There is a close relationship between the weld penetration depth and the first ionization energy of metal element in the fluxes. The regularities of metal chlorides on different materials are the same, and with the increase of first ionization energy of flux metal element in the fluxes, the penetration depth increases firstly and then decreases.

Key words: metal chloride; alternatire charging activating tungsten inert gas welding; penetration depth; ionization energy

Visual method for weld seam recognition based on multi-feature extraction and information fusion ZOU Yirong, DU Dong, ZENG Jinle, ZHANG Wenzeng (Key Laboratory for Advance Materials Processing Technology Ministry of Education, Tsinghua University, Beijing 100084, China). pp 33-36

Abstract: The complexity of welding process and the diversity of recognition object require high stability and reliability of weld seam recognition and tracking technology. These requirements can hardly be satisfied by recognition through single feature. An information fusion method based on confidence coefficient weighted probability addition is proposed: the shape feature of structured light stripe and the gray-level feature are extracted from weld seam images captured under different illumination situations. The edges of weld seam are recognized based on the two feature values, represented by probability densities of the edge and the confidence coefficients. The information fusion is real-